RSC Advances

PAPER

View Article Online
View Journal | View Issue

Cite this: *RSC Adv.*, 2015, **5**, 46955

Chitosan modification of magnetic biochar produced from *Eichhornia crassipes* for enhanced sorption of Cr(VI) from aqueous solution

Ming-ming Zhang,[ab] Yun-guo Liu,*[ab] Ting-ting Li,[ab] Wei-hua Xu,[ab] Bo-hong Zheng,[c] Xiao-fei Tan,[ab] Hui Wang,[ab] Yi-ming Guo,[d] Fang-ying Guo[ab] and Shu-fan Wang[ab]

Received 7th February 2015
Accepted 20th May 2015

DOI: 10.1039/c5ra02388b

www.rsc.org/advances

In this research, chitosan modification of magnetic biochar (CMB) was successfully prepared for effective removal of Cr(VI). Moreover, this study highlighted that the conversion of *Eichhornia crassipes* into biochar was a promising method for improved management of this highly problematic invasive species. The sorption kinetics, isotherms, thermodynamics, the effects of pH, and background electrolyte on the sorption process were investigated. The results indicated that CMB adsorbed more Cr(VI) (120 mg g^{-1}) than that of pristine biochar (30 mg g^{-1}). The sorption data could be well illustrated by pseudo-second-order and Langmuir models. Furthermore, thermodynamic parameters revealed that the sorption reaction was an endothermic and spontaneous process. The adsorption of Cr(VI) was influenced by solution pH and the maximum sorption capacity was achieved at pH 2. The background electrolyte PO_4^{3-} and SO_4^{2-} restricted the Cr(VI) sorption. These results are significant for exploring and optimizing the removal of metal ions by the CMB composite.

1. Introduction

Chromium is one of the most widespread heavy metals in the environment. However, chromium is also considered to be a major pollutant, even a priority pollutant, by the US EPA.[1] Because Cr(VI) is highly carcinogenic after long-term or high-dose exposure, Cr(VI) pollution of soil and water can pose a great threat to public health.[2] Therefore, it is urgent and necessary to take efficient measures to dispose of wastewater containing high concentrations of Cr(VI). Up to now, various technologies have been employed for Cr(VI) removal, such as ecological remediation,[3] chemical precipitation,[4] redox,[5] and adsorption.[6] Among these techniques, adsorption is regarded as the most effective and common method to remove Cr(VI) from wastewater. A variety of adsorbing materials have been applied for Cr(VI) removal through experiments, such as biochar, chitosan,[7] iron oxide.[8]

Eichhornia crassipes, a tropical species, is one of the pickerelweed family (Pontederiaceae). It has been characterized as one of the 100 most aggressive invasive species by IUCN (the International Union for Conservation of Nature) and one of the top 10 worst weeds globally.[9] *Eichhornia crassipes* grows and reproduces rapidly, leading to navigation jam, interference with irrigation, fishing and power generation.[10] In addition, *Eichhornia crassipes* can block sunlight penetration, reduce the DO concentration of water, competitively exclude submerged plants, and reduce biodiversity.[11] As a result, the conversion of *Eichhornia crassipes* into biochar afterwards application in the removal of Cr(VI) from waste water may represent a novel and attractive method for managing and controlling this highly problematic invasive species effectively.

Biochar, the product of *Eichhornia crassipes* through pyrolysis, has drawn much experiment attention recently due to its potential in resource reuse and soil improvement as well as providing renewable bioenergy and mitigating global climate change. Biochar is a stable solid, rich in carbon, and can sequester carbon in soils for thousands of years.[12] Moreover, recent studies also find biochar can be used as a low-cost sorbent to remove various contaminants from water.[13] The large specific surface area, porous structure, enriched surface functional groups and mineral components of biochar make it possible to be used as proper adsorbent to remove pollutants from aqueous solutions.[14] However, pristine biochars prepared from biomass feedstock without any treatment have relatively low heavy metal sorption capacity.[15] Therefore, various modification/activation methods, such as surface oxidization, exploration, and functionalization, have been applied to improve their performance in environmental remediation.[16–18] As previously mentioned, these modifications can add the surface sorption sites, introduce more positive charges and

[a]*College of Environmental Science and Engineering, Hunan University, Changsha 410082, PR China. E-mail: hnliuyunguo@hnu.edu.cn; Fax: +86 731 88822829; Tel: +86 731 88649208*

[b]*Key Laboratory of Environmental Biology and Pollution Control (Hunan University), Ministry of Education, Changsha 410082, PR China*

[c]*School of Architecture and Art Central South University, Changsha 410082, PR China*

[d]*School of Economics and Management, Shanghai Maritime University, 1550 Haigang Ave, Shanghai 201306, PR China*

surface functional groups on the modified surfaces, which is vital for the sorption of Cr(VI) by biochar.[2,15] Nowadays, various methods have also been developed to change the characteristics of biochar surfaces and improve their sorption ability.

Chitosan has been intensively studied previously. It is abundant, renewable, biodegradable and non-toxic in nature. Recently, chitosan has been applied to water purification and removing heavy metals from aqueous solutions.[15] It has also been used as a surface modification agent impregnated onto supporting surfaces as adsorption sites because its amine functional groups have strong bonding ability to various heavy metal ions.[15,19] So far, the research on the use of chitosan to modify the surfaces of biochars to enhance their affinity to heavy metal is limited. This combination is promising and it make full use of the advantages of biochar and chitosan, which is beneficial to bond Cr(VI).

Although the chitosan-modified biochar exhibited good sorption ability, it is difficult to be separated from aqueous solution. Therefore, an easy separation approach should be taken into account. Since exhausted biochar-based adsorbent may contain a good deal of pollutants when it is applied to treat natural water bodies. It is necessary to develop a technique to collect the pollutant-laden adsorbents from aqueous solutions to avoid secondary pollution. γ-Fe_2O_3 particles have high utility value in wastewater purification considering their low cost and easy separation. They have been successfully applied to remove organic contaminants,[20] and heavy metals.[21] However, due to their high surface energy arising from strong van der Waals forces, the γ-Fe_2O_3 nanoparticles have a tendency to form aggregates in aqueous solutions, which dramatically decrease the surface area and adsorption abilities as well as increase the cost.[22] In order to bring out the potentials of the chitosan-modified biochar and the γ-Fe_2O_3 nanoparticles, we immobilized the γ-Fe_2O_3 nanoparticles into the biochar-based adsorbent.[1,23] So chitosan-biochar/γ-Fe_2O_3 could be produced to not only enhance the sorption ability but also be magnetically collected after use.

In this study, chitosan-modified magnetic biochars were synthesized and used to remove Cr(VI) successfully. The prepared material was characterized by scanning electron microscopy (SEM), Fourier transform infrared (FTIR) analysis, X-ray photoelectron spectroscopy (XPS) analysis, (Brunauer–Emmett–Teller) BET analysis. Moreover, the relevant parameters such as pH, kinetics, and sorption isotherms were investigated to study the adsorption property of chitosan-modified magnetic biochars for Cr(VI) in aqueous solution. In addition, the competitive adsorption of the ion strength in the presence of various background electrolyte ions was also verified.

2. Materials and methods

2.1 Materials

Ferric chloride-6-hydrate ($FeCl_3 \cdot 6H_2O$) were purchased from Tianjin Kermel Reagent Co. Ltd., Tianjin, China. Chitosan (90% acetylation degree) was supplied by Sinopharm Chemical Reagent Co. Ltd., Shanghai, China. Glutaraldehyde was provided by Tianjin Guangfu Fine Chemical Research Institute, Tianjin, China. All reagents used in the experiment were of analytical reagent grade and solutions were prepared with high-purity water (18.25 MΩ cm^{-1}) from Millipore Milli-Q water purification system. The pristine biochar was produced from *Eichhornia crassipes*.

2.2 Preparation of biochar and biochar/γ-Fe_2O_3 composite

The biomass, *Eichhornia crassipes*, was dried and smashed. The treated biomass was divided into two-part. One part was immersed into the prepared $FeCl_3$ solution for 24 h. The mixture was oven-dried (80 °C). Both the $FeCl_3$ treated biomass and the pristine *Eichhornia crassipes* were pyrolyzed in a tube furnace at 600 °C in N_2 environment for 1 h. The product of non-treated biomass and pre-treated biomass were henceforth referred to as B, MB, respectively. The samples were then washed, dried (80 °C), and sieved through 100 mesh screen. At last, they were sealed to preserve before use.

2.3 Preparation of chitosan-biochar/γ-Fe_2O_3 composite

6 g of chitosan was first dissolved in 1000 mL of 2% (v/v) acetic acid. Afterwards, 6 g of biochar/γ-Fe_2O_3 composite was added and the compounds were stirred for 30 min at 40 °C. 150 mL glutaraldehyde (1% v/v) was then injected into the reaction system. After 30 min, keeping in 40 °C, NaOH solution was added dropwise into the mixtures until the pH value reached 9. In the end, the compounds were also stirred for 1 h. The detailed preparation process was shown in Fig. 1. The final product was chitosan-biochar/γ-Fe_2O_3 composite (CMB).

2.4 Materials characterization

Scanning electron microscope (SEM) images were obtained on a JEOL JSM-6700. FT-IR spectrum was measured on a

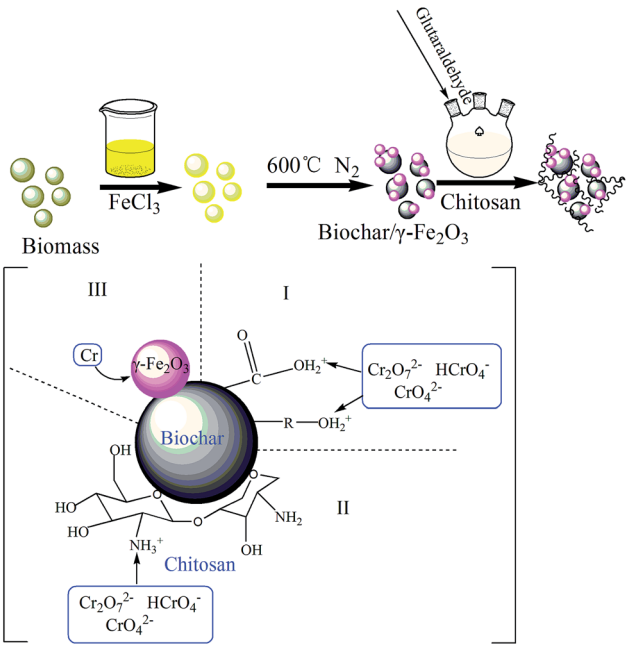

Fig. 1 Schematic representation of strategy for preparation of CMB and Cr(VI) removal by CMB.

spectrophotometer (Varian 3100, USA) using the KBr pellet technique. The XPS measurements were performed using an ESCALAB 250Xi X-ray photoelectron spectrometer (Thermo Fisher, USA). BET analysis was carried out with Tristar II 3020 (USA). The magnetic property was characterized by magnetization curve using a vibrating sample magnetometer (Lake Shore 7410, USA). The zeta potentials of CMB were measured at different pH by Zetasizer Nano ZS (ZEN3690, Malvern, UK).

2.5 Sorption experiments

All batch sorption experiments were carried out in a 150 mL Erlenmeyer flask containing 50 mL Cr(VI) solutions in an incubator shaker with a shaking speed of 150 rpm. For each treatment, 50.0 mg of adsorbent was added and shaken for specified period. The concentrations of residual Cr(VI) were determined by UV-vis spectrophotometer (Pgeneral T6, Beijing, China) at 540 nm.

Three kinds of adsorbents (B, MB, CMB) were used to study the effect of pH on Cr(VI) ions adsorption. Effects of pH (2.0–8.0) experiments were studied in 50 mL Cr(VI) solutions with the initial Cr(VI) concentration of 150 mg L^{-1} at 30 °C. The pH was adjusted to desired values by adding negligible volumes of NaOH or HCl.

Isotherm experiments were conducted with different initial Cr(VI) concentrations (20–500 mg L^{-1}) for 24 h. The experiments were carried out at different temperatures of 20, 30 and 40 °C, respectively.

Kinetic experiments were studied for different time intervals (5, 10, 30, 60 min and 2, 6, 12, 18, 24 h) 30 °C. In each study, 50.0 mg CMB was added to 50 mL Cr(VI) solution with the initial concentration of 200 mg L^{-1}.

The adsorption amount q_e (mg g^{-1}) of Cr(VI) was calculated according to eqn (1)

$$q_e = \frac{(c_0 - c_e) \times V}{m} \quad (1)$$

where c_0 and c_e were the initial and residual concentration of Cr(VI) in the solution (mg L^{-1}), respectively. V is the volume of Cr(VI) solution (mL), and m is the amount of adsorbent used (mg).

3. Results and discussion

3.1 Characterization of B, MB, CMB

The surface morphologies of the pristine biochar (B), magnetic biochar (MB) and chitosan-biochar/γ-Fe_2O_3 (CMB) were displayed in the SEM images. As shown in the Fig. 2(a), the pore structure of the pristine biochar surface was unconspicuous. However, after being disposed by $FeCl_3$, the biochar surface morphology formed plenty pore channels apparently, as displayed in Fig. 2(b). Besides, some splendent particles appeared on the surface of MB, and it may be γ-Fe_2O_3.[22] Fig. 2(c) showed the pore amount decreased distinctly. This phenomenon was explained that the biochar/γ-Fe_2O_3 was modified by coating chitosan onto it and the chitosan blocked the pore channel. Nevertheless, the sorption capacity of CMB was stronger than that of MB, which indicated that the adsorption mechanism relied on the functional groups primarily but not the surface pore structure.

The FTIR spectra of B, MB, CMB were shown in Fig. 3(a). For CMB, the peak around 3419 cm^{-1} was related to the stretching vibration of –OH and –NH groups.[24,25] The characteristic peak of CMB at 2917.5 cm^{-1} was attributed to the stretching vibration of

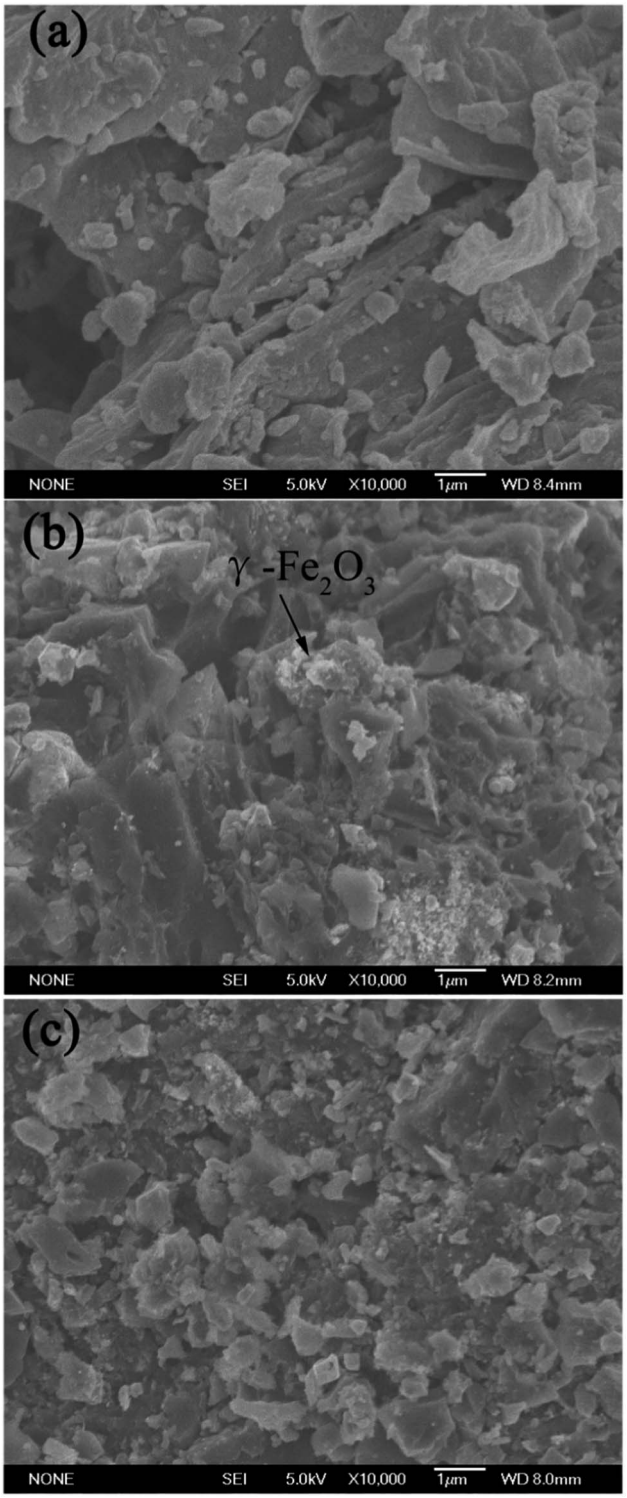

Fig. 2 SEM images of pristine biochar (a), MB (b) and CMB (c).

–CH and –CH_2. The adsorption band at 1687.5 cm^{-1} was corresponded to the C=O stretching vibrations of –NH–C=O from chitosan or the carbonyl from the carboxyl group in biochar.[19,24,26] The band at 1073.5 cm^{-1} may be connected with the C–O stretching vibration from chitosan. For CMB and MB spectra, the peaks at 576.4 and 576.8 cm^{-1} were found obviously, which was assigned to Fe–O stretching vibration. It indicated that γ-Fe_2O_3 particles were embedded in the pristine biochar. It can be observed notably from Fig. 3(a) that the types of functional groups of CMB were much more than that of pristine material. The FTIR spectra of B, MB, CMB were different with each other, which can account for the distinction of the sorption capacity of the three materials for Cr(VI) to some extent.

The FTIR spectra of CMB before and after Cr(VI) adsorption was shown in Fig. 3(b). After adsorption, a significant shift of those peaks (CMB) from 3419 cm^{-1} (–OH & –NH) to 3413.1 cm^{-1}, 1687.5 cm^{-1} (C=O of –NH–C=O) to 1589.6 cm^{-1}, and 1073.5 cm^{-1} (C–O) to 1064.2 cm^{-1} occurred perhaps. This result indicated that the main mechanism of Cr(VI) adsorption onto CMB may rely on the functional groups on the material surface.

With the purpose of gaining further information on the chemical composition of biochar and chitosan-biochar/γ-Fe_2O_3, X-ray photoelectron spectroscopy (XPS) was performed to examine the surface chemical ingredients of two materials, and the results were exhibited in Fig. 4(a), 5(a) and (b). In the XPS survey of B, three significant peaks C 1s (78.87%), O 1s (19.51%) and N 1s (1.62%) were observed. In addition to these three peaks, Fe 2p was presented in the XPS survey spectra of CMB, and the four peaks were shown as follows: C 1s (71.24%), O 1s (23.02%), N 1s (3.2%) and Fe 2p (2.54%). Comparing the two XPS survey spectra, the O/C atomic ratio and the amount of N 1s of CMB were higher than that of B, both of which were owing to the introduction of chitosan to γ-Fe_2O_3/biochar thus leading to the increase in the amount of oxygenic groups. Moreover, the existence of iron indicated that the preparation of γ-Fe_2O_3/biochar composite was successful. Fig. 5(a) expressed the C 1s XPS spectra of B, which demonstrated a considerable degree of oxidation with four components corresponding to carbon atoms in different functional groups: non-oxygenated ring C (284.5 eV), the carbon in the C–O (286.1 eV), C–N (285.2 eV) and COOH groups (290 eV).[27,28] For Fig. 5(b), the C 1s XPS spectra of CMB included four peak components too, but it represented 284.6, 286.1, 287.5, 288.7 eV, consistent with C–C, C–O, C–N, and –COOH, respectively.[29,30] The difference of the two C 1s XPS spectra was possibly due to the modification of biochar using chitosan and ferric chloride solution.

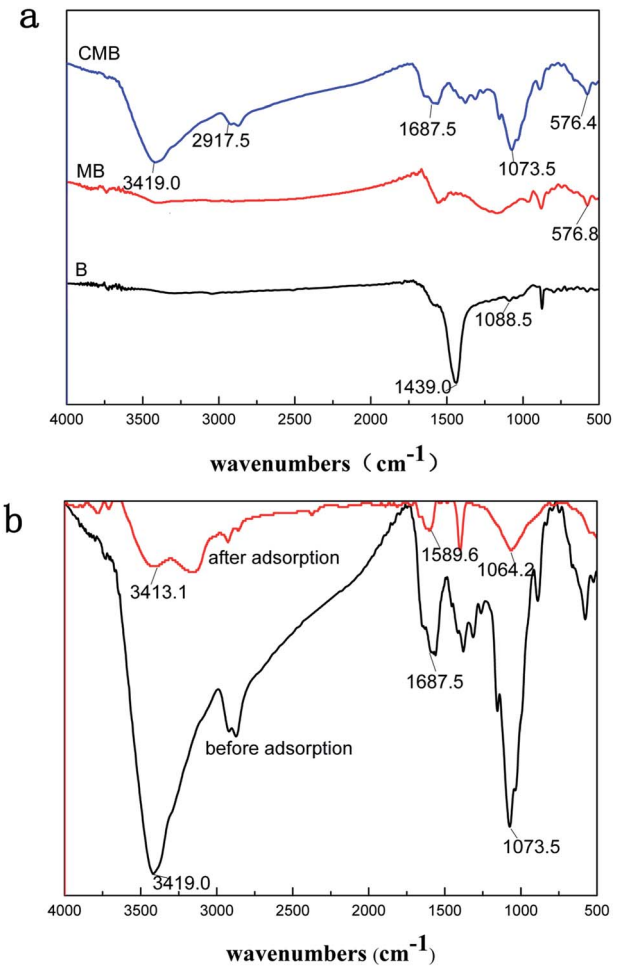

Fig. 3 (a) FTIR spectra of B, MB and CMB, (b) FTIR spectra of CMB before and after adsorption.

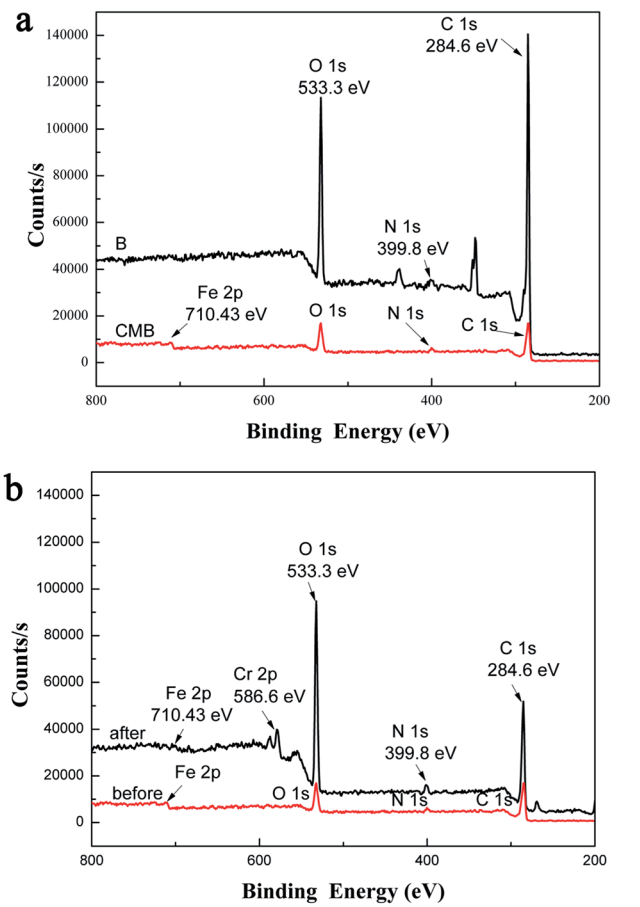

Fig. 4 (a) XPS survey spectra of B and CMB, (b) XPS survey spectra of CMB before and after adsorption.

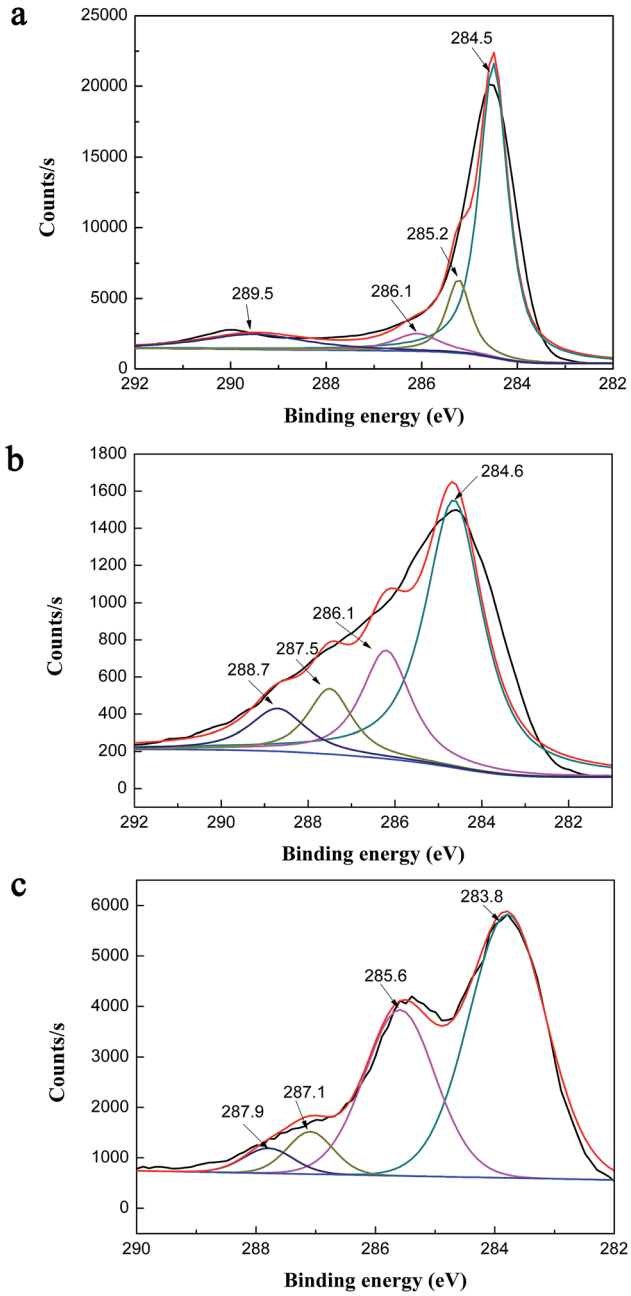

Fig. 5 The C 1s XPS spectra of B (a), CMB (b), CMB after adsorption (c).

Fig. 4(b) showed the XPS survey spectra of CMB before and after Cr(VI) adsorption. After adsorption, a new typical peak at the binding energy of 586.6 eV corresponding to Cr(VI) ions appeared,[31] which provided testify further that the process of Cr(VI) ions adsorption onto CMB took place.

Fig. 5(c) represented the C 1s XPS spectra of CMB after Cr(VI) adsorption. After Cr(VI) adsorption, there were four peaks appeared in the C 1s XPS spectra of CMB, and they were C–C (283.8 eV), C–N (285.6 eV), C–Cr (287.1 eV) and [$Cr(CO)_6$] (287.9 eV). Apparently, compared with the C 1s XPS spectra of CMB before adsorption (Fig. 5(b)), the carbon functional groups of CMB changed greatly after Cr(VI) adsorption. That is to say the carbon functional groups was the main adsorption mechanism.

Table 1 Pore distribution properties of the three materials

	BET surface area ($m^2\ g^{-1}$)	Pore volume[a] ($m^3\ g^{-1}$)	Pore size[b] (nm)
B	37.68	0.055	5.86
MB	341.09	0.20	2.36
CMB	90.78	0.064	2.81

[a] Determined at $P/P_0 = 0.99$. [b] Adsorption average pore width (4V/A by BET).

As shown in Table 1, the surface area, pore volume and pore size of B, MB and CMB existed distinction. The BET surface area of MB (341.09 $m^2\ g^{-1}$) was larger than that of B (37.68 $m^2\ g^{-1}$), and the MB possessed larger pore volume and smaller pore size than that of B. The phenomenon may be due to the process of preparing γ-Fe_2O_3/biochar, which was manufactured by immersing water hyacinth biomass into ferric chloride solution, and then changed the pore structure of pristine biochar. Compared with MB, CMB owned smaller BET surface area and pore volume, but bigger pore size, which resulted from coating chitosan on the surface of γ-Fe_2O_3/biochar and the pore channels of MB was clocked. Nevertheless, the adsorption activity of the CMB was greater than MB. These results suggested that the main mechanism for heavy metal adsorption on the CMB was not the pore structure but the surface functional group,[32] which is consistent with the SEM analysis partially.

The room-temperature magnetization hysteresis curve was measured using vibrating sample magnetometry (VSM) to study the magnetic properties of CMB. As shown in Fig. 6, the magnetic hysteresis loop was S-like curve. The saturation magnetization (M_s) of the CMB composite was 11.60 emu g^{-1}, which was sufficient to be separated from aqueous solution by a permanent magnet. The insets in Fig. 6 showed that the obtained CMB can be collected by a permanent magnet from aqueous solution. The result confirmed that CMB was magnetic

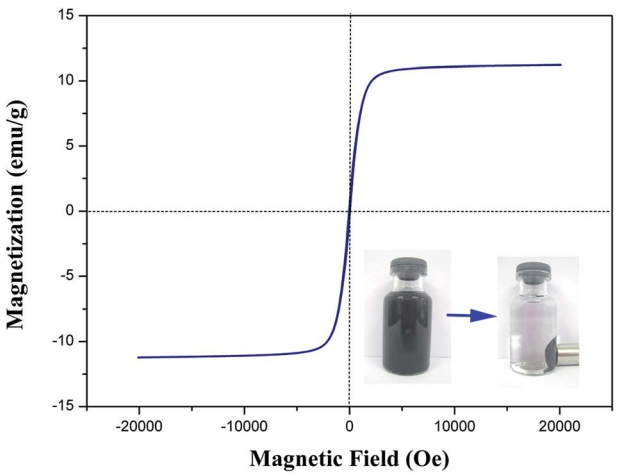

Fig. 6 Magnetization curve of CMB at room temperature (the insets show the CMB dispersed in ultrapure water and the magnetic separation).

and can potentially be used as an magnetic adsorbent to remove pollutants in liquidphase processes.

3.2 Effect of initial solution pH

The initial solution pH is a significant factor in sorption process. The removal tendencies of Cr(VI) by CMB, MB and B under different initial solution pH were presented in Fig. 8. From Fig. 8, the sorption capacities of CMB, MB and B for Cr(VI) reduced gradually with the increase of pH from 2.0 to 8.0, and the adsorption amount reached the maximum value at pH 2.0. The pH dependence of Cr(VI) was largely connected with the speciation of Cr(VI) and the surface charge of the sorbents.[28] Cr(VI) existed in different forms in aqueous solution at different pH values, such as H_2CrO_4 (aq), $Cr_2O_7^{2-}$, $HCrO_4^-$, $KCrO_4^-$, CrO_4^{2-}. $HCrO_4^-$ is the predominant Cr(VI) species at pH <6.51, while CrO_4^{2-} was predominant at pH >6.51.[28] That is to say the main speciation of Cr(VI) ions is anionic. The zeta potentials of CMB at different pH values were shown in Fig. 7. The zero point of zeta potential (pH_{ZPC}) for CMB was at pH 6.19. When the solution pH <pH_{ZPC}, the hydrated surface of CMB was protonated, which made the CMB surface potential electropositive. As a result, a remarkable electrostatic attraction occurred between the positively charged surface of the sorbent and the anionic Cr(VI) ions, which contributed to the high adsorbing capacity of Cr(VI) ions onto CMB. Nevertheless, under the solution pH >pH_{ZPC}, with the increasing of pH value, the hydrated surface of CMB was deprotonated. It caused the sorbent acquired a negative charge, which generated electrostatic repulsion that made the sorbent surface site reject the anionic Cr(VI) ions. Moreover, at pH >pH_{ZPC}, the OH^- was abundant in the solution, which can compete with Cr(VI) ions for the available adsorption sites on the surface of CMB. These are the reasons for the decrease of sorption capacity at higher pH.

From Fig. 8, we can see that the adsorption capacity of the above three materials were discrepant (CMB > MB > B). Compared with B, it was more effective for MB to eliminate Cr(VI) within a wide pH range. This could be due to the conjunct occurrence of Cr(VI) adsorption and an Fe–Cr complex reaction,[1]

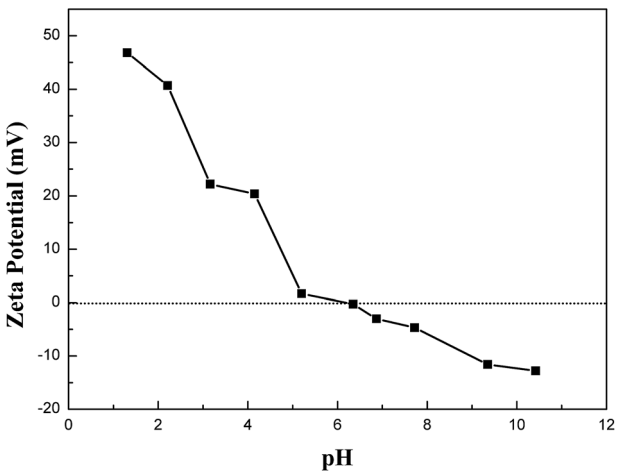

Fig. 7 Zeta potential of CMB at different solution pH.

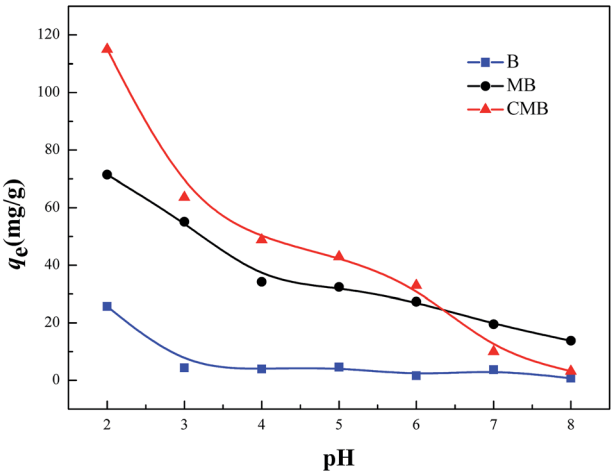

Fig. 8 Effect of the initial solution pH on adsorption of Cr(VI) by B, MB and CMB (reaction conditions: c_0 = 150 mg L^{-1}; V = 50 mL; m = 50 mg; t = 6 h; T = 30 °C).

which lowered the concentration of Cr(VI) in the solution. Besides, the sorption capacity of CMB was higher than that of MB. The reason was that the chitosan modification introduced $-NH_2$. In environment of pH <6, $-NH_2$ was protonated resulting in a stronger attraction for anionic Cr(VI) ions. The visual sorption process was displayed in Fig. 1. Moreover, in acidic environment, –COOH may be protonated, which also enhanced the sorption of anionic Cr(VI) ions on CMB. In conclusion, the new adsorbent was more effective than the pristine material on adsorbing Cr(VI) ions.

3.3 Adsorption isotherm

The sorption isotherms of Cr(VI) on the CMB were presented in Fig. 9, which showed that the adsorption capacities increased with the increasing of equilibrium concentrations, and finally approached the maximum adsorption capacities. Besides, when the initial concentration was lower than 20 mg L^{-1}, the residual Cr(VI) in the solution after adsorption by the CMB was negligible. In this study, Langmuir and Freundlich models were adopted to simulate the experimental data, and thus described the adsorption characteristics between adsorbent and Cr(VI).

The Langmuir isotherm model assumed that the adsorption process was monolayer sorption on a homogeneous sorption surface, and all the sorption sites were equal and finite, while the Freundlich isotherm model was an empirical equation for explaining heterogeneous adsorption process.[33] Both the two models were expressed as follows:

$$\text{Langmuir}: \quad q_e = \frac{q_m K_L c_e}{1 + K_L c_e} \tag{2}$$

$$R_L = \frac{1}{1 + K_L c_0} \tag{3}$$

$$\text{Freundlich}: q_e = K_F c_e^{1/n} \tag{4}$$

where c_e is the equilibrium concentration (mg L^{-1}), c_0 is the initial concentration (mg L^{-1}), q_e is the amount of Cr(VI)

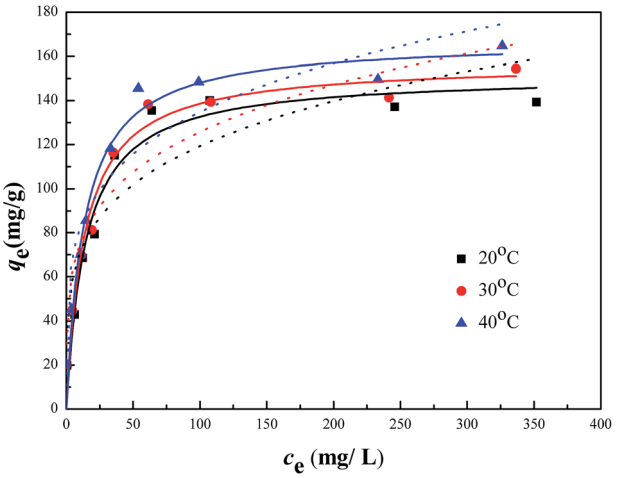

Fig. 9 Langmuir isotherm (solid line) and Freundlich isotherm (dash line) for the adsorption of Cr(VI) on CMB (reaction conditions: c_0 = 20–500 mg L^{-1}; V = 50 mL; m = 50 mg; t = 6 h; pH = 2; T = 20, 30, 40 °C).

adsorbed at equilibrium (mg g^{-1}), q_m is the maximum adsorption capacity (mg g^{-1}), R_L is the separation factor of the Langmuir. K_L is the Langmuir constant related to the affinity of the binding sites (L mg^{-1}), and K_F and n are the Freundlich constants related to the adsorption capacity and intensity, respectively.

The related parameters of the two models were listed in Table 2. It indicated that the correlation coefficient R^2 of Langmuir was higher than that of Freundlich, which suggested that the adsorption process of Cr(VI) onto CMB fit the Langmuir model better than Freundlich model. Moreover, from the equation above we can see that $0 < R_L < 1$ obviously, which manifested that the adsorption in this research was suitable for Langmuir model more adequately. It indicated that monolayer adsorption and heterogeneous surface conditions might coexist under the experimental conditions, but monolayer adsorption was more dominant.[24] Fig. 9 showed that the q_m increased with the increasing of the temperature. The values of the q_m were 151.62, 157.11, 167.31 mg g^{-1}, which was corresponding to 20, 30, 40 °C. In addition, K_L increased with the increasing of the temperature. Therefore, the adsorption process of Cr(VI) onto CMB is endothermic.[28] Comparing the maximum capacity of Cr(VI) removal with the previous study[34–38] (shown in Table 3), CMB was better than many other absorbents reported in the literature.

Table 2 Adsorption equilibrium constants obtained from Langmuir and Freundlich isotherms in the adsorption of Cr(VI) onto CMB

	Langmuir			Freundlich		
Temperature (°C)	q_{max} (mg g^{-1})	K_L (L mg^{-1})	R^2	K_F (L mg^{-1})	n	R^2
20	151.62	0.069	0.95	41.74	4.37	0.81
30	157.11	0.074	0.96	44.36	4.42	0.88
40	167.31	0.077	0.96	49.05	4.56	0.87

Table 3 Comparison of the maximum Cr(VI) adsorption capacity (q_m) of various adsorbents

Adsorbents	q_m (mg g^{-1})	References
Activated carbon derived from *Eichhornia crassipes* root biomass	36.34	34
Magnetized activated carbon	57.19	35
Saw dust activated carbon	65.8	36
Fe^0/Fe_3O_4 nanoparticles	55.64	37
Magnetic chitosan 2 (NCIM 3590)	137.27	38
Chitosan-biochar/γ-Fe_2O_3 composite (CMB)	167.31	This study

3.4 Thermodynamic analysis

Thermodynamic analysis was considered to gain an in-depth study of the adsorption process of Cr(VI) onto CMB. Thermodynamic parameters such as Gibbs free energy ΔG^0, enthalpy ΔH^0, entropy ΔS^0 were calculated by the following equations:

$$\Delta G^0 = -RT \ln K \quad (5)$$

$$\ln K = -\frac{\Delta G^0}{RT} = -\frac{\Delta H^0}{RT} + \frac{\Delta S^0}{R} \quad (6)$$

where K is the adsorption equilibrium constant. T (K) is the absolute temperature, and R (8.314 J mol^{-1} K^{-1}) is the gas constant. ΔH^0 and ΔS^0 could be calculated from the slope and intercept of ln K *versus* $1/T$. The results of the thermodynamic parameters were shown in Table 4.

From Table 4, we can see that the negative values of the ΔG^0 (−19.97 kJ mol^{-1} at 293.15 K, −20.82 kJ mol^{-1} at 303.15 K, and −21.59 kJ mol^{-1} at 313.15 K) became more negative with the rising temperature, which indicated that the process of the adsorption was spontaneous in nature and the degree of the reaction spontaneity increased with the rising temperature.[24] Furthermore, the positive value of ΔH^0 (3.67 kJ mol^{-1}) demonstrated that the sorption was endothermic, which was consistent with the result of the adsorption isotherm. Finally, the positive value of ΔS^0 (80.68 J K^{-1} mol^{-1}) probably reflected the growth of randomness at the solid/solution interface during the adsorption process and a good affinity of Cr(VI) onto CMB.[24] Moreover, some structural changes of adsorbate and adsorbent may also occur during the adsorption process. In conclusion, the sorption of Cr(VI) onto CMB is an endothermic and spontaneous process.

3.5 Kinetic studies

The effect of the contact time on CMB adsorption capacity was shown in Fig. 10(a). The removal capacity of CMB on Cr(VI) markedly increased in the first 120 min, which was owing to the existence of plentiful active sites on the adsorbent surface. And then, the trend rose slowly until the adsorption equilibrium was reached within 360 min. The reason for the slow adsorption process was that the majority of active surface sites were occupied by Cr(VI), and there were insufficient binding sites for the material adsorbing Cr(VI).

Table 4 Thermodynamic parameters for the adsorption of Cr(VI) by CMB

ΔH^0 (kJ mol^{-1})	ΔS^0 (J K^{-1} mol^{-1})	ΔG^0 (kJ mol^{-1})		
		20 °C	30 °C	40 °C
3.67	80.68	−19.97	−20.82	−21.59

Table 5 Pseudo-first-order model and pseudo-second-order model parameters for Cr(VI) adsorption on CMB

Pseudo-first-order model			Pseudo-second-order model		
k_1 (min^{-1})	q_e (mg g^{-1})	R^2	k_2 (g mg^{-1} min^{-1})	q_e (mg g^{-1})	R^2
4.71×10^{-4}	31.95	0.65	1.74×10^{-4}	132.28	0.99

To investigate the mechanism of adsorption, kinetic models were applied to explain the experimental data. In this research, two different models were applied and illustrated as follows:

The pseudo-first-order model:

$$\log(q_e - q_t) = \log q_e - \frac{k_1}{2.303} t \quad (7)$$

The pseudo-second-order model:

$$\frac{t}{q_t} = \frac{t}{q_e} + \frac{1}{k_2 q_e^2} \quad (8)$$

where q_e and q_t are the adsorption amounts (mg g^{-1}) at equilibrium and at time t, respectively. k_1 is the pseudo-first-order rate constant (min^{-1}), k_2 is the pseudo-second-order rate constant (g mg^{-1} min^{-1}).

Contact time effect and pseudo-second-order sorption kinetics were shown in Fig. 10(a) and (b), respectively. The kinetic parameters calculated from the two models were listed in Table 5. Obviously, the correlation coefficient R^2 of the pseudo-second-order model was more than 0.99, which was higher than that of the pseudo-first-order model. Besides, the calculated q_e agreed very well with the experimental data. The result indicated that the kinetic data for the adsorption process fit the pseudo-second-order model, which showed that the mechanism of Cr(VI) sorption by the CMB depended on the rate-controlling step due to chemical sorption.[28,39,40]

3.6 Effect of background electrolyte on Cr(VI) removal

Fig. 11 showed the effect of background electrolyte on the Cr(VI) adsorption onto the CMB at pH 2 in 0.01 mol L^{-1} NaCl, $Ca(NO_3)_2$, $CaCl_2$, Na_3PO_4, Na_2SO_4 solution, respectively. As shown in Fig. 11, all the five electrolyte have the influence of different levels, which is reflected by the following sequence of the Cr(VI) sorption capacity: NaCl > $Ca(NO_3)_2$ > $CaCl_2$ > Na_3PO_4 > Na_2SO_4. NaCl, $Ca(NO_3)_2$ and $CaCl_2$ had less effect on the removal of Cr(VI) than the other two electrolytes. Na_3PO_4 and Na_2SO_4 inhibited the Cr(VI) sorption distinctly and reduced the

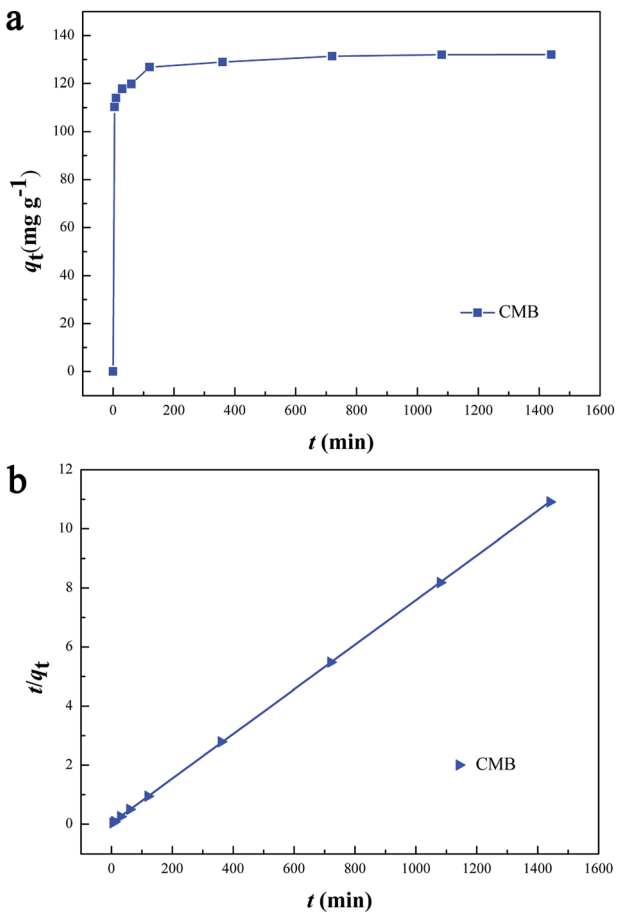

Fig. 10 (a) Effect of contact time of Cr(VI) adsorption onto CMB and (b) pseudo-second-order sorption kinetics of Cr(VI) adsorption onto CMB (reaction conditions: $c_0 = 200$ mg L^{-1}; $V = 50$ mL; $m = 50$ mg; pH = 2; $T = 30$ °C).

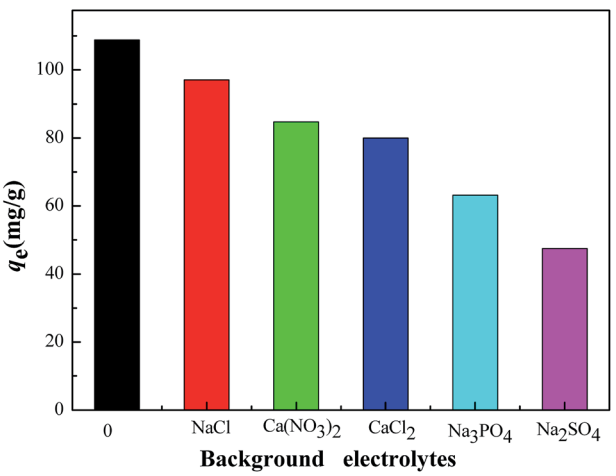

Fig. 11 Effect of background electrolyte (NaCl, $Ca(NO_3)_2$, $CaCl_2$, Na_3PO_4, Na_2SO_4) on the Cr(VI) adsorption by CMB. (Reaction conditions: electrolyte concentration 0.01 mol L^{-1}; Cr(VI) concentration $c_0 =$ 150 mg L^{-1}; $V = 50$ mL; $m = 50$ mg; $T = 30$ °C; pH = 2).

adsorption capacity from 108.84 mg g^{-1} to 63.17 mg g^{-1}, 47.49 mg g^{-1}, respectively. What can explain this phenomenon is the competition mechanism. As for NaCl, $Ca(NO_3)_2$, $CaCl_2$, Cl^- and NO_3^- are monovalent anions, and they may slightly compete with the chromium anion for the positive charge sorption sites on the CMB surface. However, the PO_4^{3-} and the SO_4^{2-} from Na_3PO_4 and Na_2SO_4 are multivalent anions, which could compete with $Cr_2O_7^{2-}$, $HCrO_4^-$, $KCrO_4^-$, CrO_4^{2-} for more available sorption sites of the CMB. The study of the effect of background electrolyte on Cr(VI) removal demonstrated that electrostatic force is one possible sorption mechanism for the removal of Cr(VI) onto CMB.

4. Conclusions

In this work, chitosan-biochar/γ-Fe_2O_3 was successfully synthesized and applied to remove Cr(VI) from the wastewater. The magnetic composite possessed a high Cr(VI) adsorption capacity and can be easily separated from the solution, by combining the superiority of chitosan, biochar and γ-Fe_2O_3. The features of the novel material were low operating cost, easily available biomass resource, magnetic, abundant functional groups, and the remission of the invasive species (*Eichhornia crassipes*). Moreover, the adsorption capacity was affected by the solution pH and the maximum Cr(VI) adsorption capacity was found at pH 2. The Langmuir isotherm model fit the experimental data very well. It indicated that monolayer adsorption is the main mechanism. The maximum adsorption capacity obtained from Langmuir model were 139.21, 154.37 and 164.71 mg g^{-1} at 20, 30 and 40 °C, respectively. Kinetic studies showed that the pseudo-second-order model illustrated the best description for the adsorption process of Cr(VI) onto CMB, which suggested the rate limiting step may be chemisorption. The analysis of thermodynamic showed that the sorption of Cr(VI) onto CMB was an endothermic and spontaneous process. Cr(VI) adsorption can be restrained by some multivalent anions, such as PO_4^{3-} and SO_4^{2-}. Moreover, the FTIR and XPS analysis illustrated that the functional groups changed after modification, resulting in enhancing the sorption ability for Cr(VI). In conclusion, the effective and environmental friendly absorbent (CMB) will have broad applications in the removal of Cr(VI) from wastewater.

Acknowledgements

The authors would like to thank financial support from the National Natural Science Foundation of China (Grant no. 41271332, 51478470 and 51108167).

References

1 L. Tang, G.-D. Yang, G.-M. Zeng, Y. Cai, S.-S. Li, Y.-Y. Zhou, Y. Pang, Y.-Y. Liu, Y. Zhang and B. Luna, *Chem. Eng. J.*, 2014, **239**, 114–122.
2 Y. S. Shen, S. L. Wang, Y. M. Tzou, Y. Y. Yan and W. H. Kuan, *Bioresour. Technol.*, 2012, **104**, 165–172.
3 Q. Zhou and Y. Song, *Remediation of contaminated soils: principles and methods*, Science Press, Beijing, 2004.
4 X. Zhou, T. Korenaga, T. Takahashi, T. Moriwake and S. Shinoda, *Water Res.*, 1993, **27**, 1049–1054.
5 Y. Pang, G.-M. Zeng, L. Tang, Y. Zhang, Y.-Y. Liu, X.-X. Lei, M.-S. Wu, Z. Li and C. Liu, *Bioresour. Technol.*, 2011, **102**, 10733–10736.
6 D. Mohan and C. U. Pittman Jr, *J. Hazard. Mater.*, 2006, **137**, 762–811.
7 Y. A. Aydın and N. D. Aksoy, *Chem. Eng. J.*, 2009, **151**, 188–194.
8 P. Xu, G. M. Zeng, D. L. Huang, C. L. Feng, S. Hu, M. H. Zhao, C. Lai, Z. Wei, C. Huang, G. X. Xie and Z. F. Liu, *Sci. Total Environ.*, 2012, **424**, 1–10.
9 F. Zhang, X. Wang, D. Yin, B. Peng, C. Tan, Y. Liu, X. Tan and S. Wu, *J. Environ. Manage.*, 2015, **153**, 68–73.
10 Y. Huang, S. Li, J. Chen, X. Zhang and Y. Chen, *Appl. Surf. Sci.*, 2014, **293**, 160–168.
11 I. Guerrero-Coronilla, L. Morales-Barrera and E. Cristiani-Urbina, *J. Environ. Manage.*, 2015, **152**, 99–108.
12 M. Zhang, B. Gao, Y. Yao, Y. Xue and M. Inyang, *Sci. Total Environ.*, 2012, **435–436**, 567–572.
13 Y. Yao, B. Gao, H. Chen, L. Jiang, M. Inyang, A. R. Zimmerman, X. Cao, L. Yang, Y. Xue and H. Li, *J. Hazard. Mater.*, 2012, **209–210**, 408–413.
14 X. F. Tan, Y. G. Liu, G. M. Zeng, X. Wang, X. J. Hu, Y. L. Gu and Z. Z. Yang, *Chemosphere*, 2015, **125**, 70–85.
15 Y. Zhou, B. Gao, A. R. Zimmerman, J. Fang, Y. Sun and X. Cao, *Chem. Eng. J.*, 2013, **231**, 512–518.
16 Y. Xue, B. Gao, Y. Yao, M. Inyang, M. Zhang, A. R. Zimmerman and K. S. Ro, *Chem. Eng. J.*, 2012, **200–202**, 673–680.
17 M. Zhang, B. Gao, Y. Yao, Y. Xue and M. Inyang, *Sci. Total Environ.*, 2012, **435–436**, 567–572.
18 W. Zhang, L. Wang and H. Sun, *Chemosphere*, 2011, **85**, 1306–1311.
19 D. Kołodyńska, *Chem. Eng. J.*, 2011, **173**, 520–529.
20 T. Phenrat, Y. Liu, R. D. Tilton and G. V. Lowry, *Environ. Sci. Technol.*, 2008, **43**, 1507–1514.
21 Y. Pang, G. Zeng, L. Tang, Y. Zhang, Y. Liu, X. Lei, Z. Li, J. Zhang, Z. Liu and Y. Xiong, *Chem. Eng. J.*, 2011, **175**, 222–227.
22 M. Zhang, B. Gao, S. Varnoosfaderani, A. Hebard, Y. Yao and M. Inyang, *Bioresour. Technol.*, 2013, **130**, 457–462.
23 B. Chen, Z. Chen and S. Lv, *Bioresour. Technol.*, 2011, **102**, 716–723.
24 T.-T. Li, Y.-G. Liu, Q.-Q. Peng, X.-J. Hu, T. Liao, H. Wang and M. Lu, *Chem. Eng. J.*, 2013, **214**, 189–197.
25 Y. Ren, H. A. Abbood, F. He, H. Peng and K. Huang, *Chem. Eng. J.*, 2013, **226**, 300–311.
26 X. Dong, L. Q. Ma and Y. Li, *J. Hazard. Mater.*, 2011, **190**, 909–915.
27 S. Hou, S. Su, M. L. Kasner, P. Shah, K. Patel and C. J. Madarang, *Chem. Phys. Lett.*, 2010, **501**, 68–74.
28 H. Wang, Y. G. Liu, G. M. Zeng, X. J. Hu, X. Hu, T. T. Li, H. Y. Li, Y. Q. Wang and L. H. Jiang, *Carbohydr. Polym.*, 2014, **113**, 166–173.

29 C. Shan, H. Yang, D. Han, Q. Zhang, A. Ivaska and L. Niu, *Langmuir*, 2009, **25**, 12030–12033.
30 L. Q. Xu, D. Wan, H. F. Gong, K. G. Neoh, E. T. Kang and G. D. Fu, *Langmuir*, 2010, **26**, 15376–15382.
31 Q. Cheng, C. Li, L. Xu, J. Li and M. Zhai, *Chem. Eng. J.*, 2011, **173**, 42–48.
32 T. Chen, Y. Zhang, H. Wang, W. Lu, Z. Zhou, Y. Zhang and L. Ren, *Bioresour. Technol.*, 2014, **164**, 47–54.
33 X. J. Hu, J. S. Wang, Y. G. Liu, X. Li, G. M. Zeng, Z. L. Bao, X. X. Zeng, A. W. Chen and F. Long, *J. Hazard. Mater.*, 2011, **185**, 306–314.
34 A. K. Giri, R. Patel and S. Mandal, *Chem. Eng. J.*, 2012, **185–186**, 71–81.
35 S. Nethaji, A. Sivasamy and A. B. Mandal, *Bioresour. Technol.*, 2013, **134**, 94–100.
36 E. A. Oliveira, S. F. Montanher, A. D. Andrade, J. A. Nóbrega and M. C. Rollemberg, *Process Biochem.*, 2005, **40**, 3485–3490.
37 A. Rao, A. Bankar, A. R. Kumar, S. Gosavi and S. Zinjarde, *J. Contam. Hydrol.*, 2013, **146**, 63–73.
38 N. N. Thinh, P. T. Hanh, T. T. Ha le, N. Anh le, T. V. Hoang, V. D. Hoang, H. Dang le, N. V. Khoi and T. D. Lam, *Mater. Sci. Eng., C*, 2013, **33**, 1214–1218.
39 D. Kołodyńska, R. Wnętrzak, J. J. Leahy, M. H. B. Hayes, W. Kwapiński and Z. Hubicki, *Chem. Eng. J.*, 2012, **197**, 295–305.
40 Z. Sun, Y. Liu, Y. Huang, X. Tan, G. Zeng, X. Hu and Z. Yang, *J. Colloid Interface Sci.*, 2014, **434**, 152–158.